Stress Distribution in the Western India-Eurasia Collision Zone: A Region of Varying Stress Fields in a Compressional Regime

R. Arun Prasath[1], Brijesh Bansal[1], and MITHILA VERMA[1]

[1]Ministry of Earth Sciences, New Delhi, India

November 21, 2022

Abstract

The western India-Eurasia collision zone (IECZ) has experienced devastating earthquakes in the past century and continues to be seismically active. However, the Stress regime and Seismotectonics of the region remains poorly understood. In view of this, we carried out iterative, joint stress inversions of 245 well-constrained earthquake focal mechanisms to constrain the stress regime and its spatial variability in the region and dwell upon their implications for earthquake generation. Salient new findings from the study are, (i) the Kangra-Chamba-Kishtwar region shows arc-oblique horizontal maximum compressive stress (sigma 1, WSW-ENE) in contrast to arc-normal (NNE-SSW) in other regions of the Himalaya, (ii) the Kashmir earthquake sequence (in 2005) and its epicentral region i.e. the Hazara Syntaxis show similar stress patterns with that of the Central Himalaya, (iii) Nanga Parbat Syntaxis experiences pure extension, and (iv) Kaurik Chango Rift, with N-S trending sigma 1, probably extends deep into the Karakoram fault. Based on these findings, we categorize the region into six state of stress fields consistent with geology and plate motion models. The magnitudes for these stress fields show a decreasing trend from 0.90 in the southeast (Garhwal-Kumaun-Shimla) to 0.46 in the northwest (Hazara Syntaxis) and 0.39 in the northeast (Karakoram) suggesting multiple tectonic forces in northwestern and northeastern regions. The study reveals heterogeneity in the stress field within the western IECZ, induced by tectonic forces and structural variability.

Hosted file

supplementary table s3.docx available at https://authorea.com/users/531414/articles/597637-stress-distribution-in-the-western-india-eurasia-collision-zone-a-region-of-varying-stress-fields-in-a-compressional-regime

Hosted file

supplementary table s2.docx available at https://authorea.com/users/531414/articles/597637-stress-distribution-in-the-western-india-eurasia-collision-zone-a-region-of-varying-stress-fields-in-a-compressional-regime

Hosted file

supplementary table s1.docx available at https://authorea.com/users/531414/articles/597637-stress-distribution-in-the-western-india-eurasia-collision-zone-a-region-of-varying-stress-fields-in-a-compressional-regime

1   **Stress Distribution in the Western India-Eurasia Collision Zone: A Region of**

2   **Varying Stress Fields in a Compressional Regime**

3   R. Arun Prasath*, Brijesh K. Bansal, Mithila Verma

4   Ministry of Earth Sciences, Seismology Division, Prithvi Bhavan, Lodhi Road, New Delhi,

5   India.

6   *devanthran@hotmail.com | arun.devanthran@nic.in

7

8

9

10

11

12

13

14

15

16

17

18

19

20

Abstract

The western India-Eurasia collision zone (IECZ) has experienced devastating earthquakes in the past century and continues to be seismically active. However, the Stress regime and Seismotectonics of the region remains poorly understood. In view of this, we carried out iterative, joint stress inversions of 245 well-constrained earthquake focal mechanisms to constrain the stress regime and its spatial variability in the region and dwell upon their implications for earthquake generation. Salient new findings from the study are, (i) the Kangra-Chamba-Kishtwar region shows arc-oblique horizontal maximum compressive stress ($\sigma 1$, WSW-ENE) in contrast to arc-normal (NNE-SSW) in other regions of the Himalaya, (ii) the Kashmir earthquake sequence (in 2005) and its epicentral region i.e. the Hazara Syntaxis show similar stress patterns with that of the Central Himalaya, (iii) Nanga Parbat Syntaxis experiences pure extension, and (iv) Kaurik Chango Rift, with N-S trending $\sigma 1$, probably extends deep into the Karakoram fault. Based on these findings, we categorize the region into six state of stress fields consistent with geology and plate motion models. The magnitudes for these stress fields show a decreasing trend from 0.90 in the southeast (Garhwal-Kumaun-Shimla) to 0.46 in the northwest (Hazara Syntaxis) and 0.39 in the northeast (Karakoram) suggesting multiple tectonic forces in northwestern and northeastern regions. The study reveals heterogeneity in the stress field within the western IECZ, induced by tectonic forces and structural variability.

1. Introduction

India-Eurasia Collision Zone (IECZ), predominantly compressional in nature, was formed by a continent-continent collision during the Eocene period, not more than 57 Ma ago

47   (Molnar & Tapponnier, 1977; Leech et al., 2005). The region has a diverse tectonic setting

48   spanning the great Himalayan intra-crustal thrusts to the normal faults in the Tethyan-Tibetan

49   regions and numerous transverse structures of the region (Molnar & Tapponnier, 1977;

50   Tapponnier et al., 1981). The IECZ has experienced a number of destructive earthquakes such

51   as, M_w 8.2 Bihar-Nepal earthquake (1934), M_w 7.6 Kashmir earthquake (2005) and M_w 7.8

52   Nepal earthquake (2015) owing to the continuing plate convergence of 37-44 mm/yr (Arora et

53   al., 2017; Avouac et al, 2006; Banerjee & Bürgmann, 2002; Sapkota et al., 2013). In the

54   western IECZ, the majority of the earthquakes occur along a linear trend known as Himalayan

55   Seismic Belt (HSB). The HSB is positioned around two intra-crustal boundary thrusts, viz., the

56   Main Central Thrust and the Main Boundary Thrust. Besides, two major structures in the Tibetan

57   Plateau, viz., the Karakoram Fault, a dextral fault and the Kaurik Chango Rift (KCR), a

58   transverse and trans-tensional structure located between Karakoram Fault and the Himalayan

59   wedge are also experiencing moderate earthquake activity (Gahalaut & Kundu, 2012; Ni &

60   Barazangi, 1984).

61   Imaging the crustal stress field using double-couple earthquake focal mechanisms

62   (FM) could provide crucial information to understand the tectonic stress regime, its variation

63   and the role of local and transverse tectonics that are responsible for earthquake generation

64   and help constrain the kinematics, earthquake nucleation processes and hazard estimation. A

65   few earlier studies have attempted to image the stress field of the region utilizing the available

66   FM solutions in small patches (Gahalaut & Rao, 2009; Mahesh et al., 2015; Prasath et al.,

67   2017; Yadav et al., 2016; Yadav et al., 2017). However, some of these studies were based on

68   the FM solutions of micro-earthquakes of magnitudes 1.5<M<3.0 with low azimuthal

69   coverage and less polarity readings. Recent advancements in the seismic networks of this

70   region and advanced inversion techniques developed in the 21st century have helped in

71   achieving more stable and reliable moment tensor solutions as small as M$_w$ 3.0 (D'Amico,

72   2018; see also Prasath et al., 2017). In the present study, we utilize a catalog of 245 reliable

73   FM solutions for earthquakes with magnitudes of 3.0≤M≤7.6 to image the current stress field,

74   its variability and to understand the dominant forces and Seismotectonics of the western IECZ

75   (Figures 1 and 2; Supplementary Tables S1-S3).

76

2. Structural Framework

78   The structural framework of the study area is highly complex, which comprises of the

79   western Himalayan Syntaxial zone, Western Himalaya, Garhwal-Kumaun sector of the

80   Central Himalaya and the western Tibetan region. The Himalayan wedge (western and central

81   Himalaya), which is sandwiched between the southern Tibet in the north and the Indo

82   Gangetic plains in the south, comprises of major intra-crustal boundary faults viz., (i) the

83   Himalayan Frontal Thrust (HFT), (ii) Main Boundary Thrust (MBT), (iii) Main Central Thrust

84   (MCT), (iv) Southern Tibetan Detachment (STD) and (v) Indus Tsangpo Suture (ITS) (Figure

85   1) (Gansser, 1964). These northward dipping structures are dividing the region into different

86   litho-tectonic zones viz., (from south to north), Sub Himalaya (SH), Lesser Himalaya (LH),

87   Higher Himalayan Crystallines (HHC) and Tethyan Himalaya (TH) (Figure 1) (Gansser,

88   1964). Other significant structural features in the Himalayan wedge are the Kishtwar Window

89   (KW), the Kullu-Larji-Rampur Window (KLRW) and the Almora Klippen (AK) (Figure 1).

90   The Western Himalayan Syntaxial zone comprising of (i) Salt Range Thrust (SRT, an

91   equivalent to the HFT), (ii) Main Mantle Thrust (MMT, *aka* Shyok Suture zone, which is an

4

92   equivalent to the ITS) and (iii) Main Karakorum Thrust (MKT). This zone also includes

93   Nanga Parbat Syntaxis in its northwest and Hazara Syntaxis in its core, where the M_w 7.6

94   Kashmir earthquake of 2005 had occurred. The other significant geological features in this

95   part of the region are (i) Balakot Bagh Fault (BBF) and (ii) Jhelum Fault (JF) and (iii) the

96   Srinagar Basin (SB), in which the Srinagar basin demonstrate very less seismicity in

97   comparison to the adjacent regions (Figure 1).

98   The major faults of the Himalayan wedge are sole to a shallow and north dipping basal

99   detachment aka the Main Himalayan Thrust (MHT) located between the depths of 10 and 20

100   km beneath the region (Ni & Barazangi, 1984). The MHT is locked along the plate interface

101   with 100-120 km coupling width, however the Syntaxial zone have the broader width of 140-

102   180 km (Li et al., 2018 and references there in).

103   The northeastern part of the study region i.e. the western Tibet is occupied by the

104   Karakoram Fault (KF), a dextral fault of ~800 km long, dividing the Tibetan plateau into two

105   parts (Leech, 2008; Phillips et al., 2004). This region also comprises of two major sinistral

106   faults viz., Longmu Gozha Fault (LGF, an equivalent to the MKT), and Karakax Fault (KXF)

107   (Figure 1). The convergence rate along the Leh-Ladakh region is 17.8±1 mm/yr., while the

108   Western Himalaya and the Garhwal-Kumaun sector of the Central Himalaya are having less

109   convergence, at the rate of ~15 mm/yr. (Banerjee et al., 2008; Banerjee & Bürgmann, 2002;

110   Jade et al., 2014, 2017; Mondal et al., 2016 and references there in). South of the KF, lies the

111   Kaurik Chango Rift (KCR), a transverse structure, which is suggested to have a seismogenic

112   relationship to the earthquakes of the Garhwal Himalaya located south of this rift (Arora et

113   al., 2012). The KCR have also been linked to an inherited basement structure that exists

114 beneath the Garhwal Himalaya i.e. the Delhi-Haridwar Ridge (DHR), trending NE-SW,

115 almost perpendicular to the major Himalayan structures.

116

117 **3. Data and Methodology**

118 The FM data have been compiled from 25 different sources comprising of various

119 literature that also includes the solutions from Global Centroid Moment Tensor (GCMT)

120 catalog (Baranowski et al., 1984; Chandra et al., 1974; Das Gupta et al., 1982; Dziewonski et

121 al., 1981; Ekström et al., 2012; Gahalaut & Rao, 2009; Hazarika et al., 2017; Kanna et al.,

122 2018; Mahesh et al., 2015; Negi et al., 2017; Parija et al., 2018; Paul et al., 2018; Prasath et

123 al., 2017; Ram et al., 2005; Rastogi, 1974; Singh et al., 2018; Srinagesh et al., 2018; Kumar et

124 al., 2009; Molnar & Chen, 1983; Molnar & Lyon-Caent, 1989; Srivastava et al., 1987; Tandon

125 & Srivastava, 1975; Verma and Sekhar, 1986; Verma et al., 2015; Yadav et al., 2016)

126 (Supplementary Tables S1-S3). Initially, more than 320 solutions were considered, however

127 only 245 FM solutions which passed our quality criteria have been chosen. The primary

128 criterion was to select crustal earthquakes with magnitude M≥3.0. Majority of those (N=210)

129 are located in the upper crust in the 0-25 km depth range with maximum depth being 66 km.

130 Due weightage was given to quality of the solutions, viz., (i) the technique used, (ii) the

131 availability of local network data, and (iii) well constrained results with minimal errors. In the

132 instance of multiple solutions with moment tensors against other type of FM solutions such as

133 FOCMEC and INVRAD, the moment tensor solutions were preferred due to their reliability

134 and better constraints. Also, in case of multiple solutions with similar techniques, only those

135 obtained using local networks and with larger number of station records were chosen; e.g., in

136 the case of the M_L 5.5 Dharamshala earthquake (1986) which has multiple solutions, the one

6

137   that utilized the local network data and has better azimuthal coverage was chosen (Ram et al.,

138   2005). In the resultant catalog of 245 solutions, 186 are from the moment tensor inversion

139   techniques, while the remaining are from a combination of one or more of the following, (i)

140   Body-wave synthetic matching, (ii) P-wave first motion polarity readings and (iii) Amplitude

141   inversions.

142   We used an iterative joint inversion technique to obtain stress and fault orientations,

143   which is based on the inversion method of Michael (1987). The inversion was performed in

144   MATLAB environment using the program STRESSINVERSE (Vavryčuk, 2014). It produces

145   three principle stress directions (σ1- σ3) and stress magnitude *aka* shape ratio 'R' (R-value)

146   using the following relation (Gephart & Forsyth, 1984).

147        $$R = \frac{(\sigma1 - \sigma2)}{(\sigma1 - \sigma3)} \qquad\qquad\qquad \text{- (1)}$$

148   The program makes use of both the nodal planes of each FM solutions and identifies

149   the faults using an instability analysis. The instability analysis was performed with the

150   nominal values of 0 to 1 and the maximum value being the maximum possibility for being

151   ruptured. While carrying out the instability analysis, the friction coefficient (FC) 'μ' is

152   estimated. The identified faults were plotted on a Mohr circle diagram to identify the optimal

153   planes.

154   To address the local variations in stress field, we have divided the region into nine

155   seismotectonic zones based on its geology, tectonics, faulting type and geographical

156   proximity of the FM solutions, viz., Garhwal-Kumaun Himalaya (GKH), Shimla Hills,

157   Kangra-Chamba, Kishtwar, epicentral region of the Kashmir earthquake (Hazara Syntaxis),

158   Nanga Parbat Syntaxis, Northwest KF, Southeast KF and KCR (Figure 2). Besides, the

159   inversion has also been performed separately for the aftershocks of the 2005 Kashmir

160   earthquake to understand its stress pattern.

161   Since the available FM solutions show a spatial variability, we further categorized the

162   data into two sets, viz., (i) HSB with thrust-type solutions, and (ii) north of HSB with strike-

163   slip and normal fault type solutions. Further, we performed an inversion for the complete

164   dataset (Table 1). For each inversion, we compute the best-fitting stress field vectors, viz.,

165   compressive ($\sigma1$), intermediate ($\sigma2$) and tensile ($\sigma3$), the shape ratio *aka* the stress magnitude

166   (R-value), Coefficient of Friction (FC) and Optimally Oriented Fault planes (hereafter

167   referred to as optimal planes), which governs the susceptibility of a fault to be ruptured under

168   the given stress conditions.

169

4. Results and Discussion

171   The overall stress inversion for the western IECZ shows a compressional tectonic

172   regime with dominant $\sigma1$ oriented towards NE-SW and R-value of 0.7 (Figure 3, Table 1, and

173   Supplementary Figure S1). However, the zone-wise results obtained show varying tectonic

174   stress regimes and orientations for different zones suggesting significant heterogeneity in the

175   stress field of the region. These are explained below.

4.1 Compressional stress regime

177   The GKH and Shimla regions show compressional stress regime with sub-horizontal

178   and arc-normal $\sigma1$ (NE-SW), in good agreement with the direction of relative motion of

179   Indian plate (Figure 3). The high R-value of 0.93 and 0.85 for GKH and Shimla, respectively

180   show that the generation of seismogenic stress in these regions is controlled predominantly by

181   σ1 (Table 1). The plunge of σ1 for both the regions are found to be 19º, consistent with the

182   preferred nodal planes of optimal planes (25º and 26º, respectively), which suggests active

183   deformation along the mid-crustal ramp of the detachment having a shallow dip of <25º (Ni &

184   Barazangi, 1984). Besides, the low FC obtained for both the regions (0.66 and 0.7 for GKH

185   and Shimla, respectively) along with low b-value and the occurrence of low-velocity zones

186   reported in the literature suggest the presence of fluids and their role in earthquake generation

187   processes (Mahajan et al., 2010; Prasath et al., 2017; Rawat et al, 2014).

188   Despite having similar (compressional) stress regimes, the Kangra-Chamba and

189   Kishtwar regions show arc-oblique principle compressive stress (σ1≠90º to the Himalayan

190   Arc, ~65º in this context) in comparison to the arc-normal principle compressive stress

191   (σ1=90º to the Arc) for GKH and Shimla regions (Figure 3). Further, the moderate R-value

192   (0.62 and 0.78, respectively) and relatively high FC (0.85 and 1.2) estimated for these regions

193   are different than the GKH and Shimla regions (Table 1). Previous studies based on the

194   erosional rates, thermo-chronology, topography, geomorphogical indicators and earthquake

195   moment tensors have proposed the 77º N longitude, which separates GKH and Shimla Hills

196   zones from Kangra-Chamba and Kishtwar zones, as a transition between contradictory

197   tectonic settings on either side (Eugster et al., 2018; Nennewitz et al., 2018). Also, Seeber &

198   Pêcher (1998) proposed that the India-Eurasia convergence is arc-normal in the central

199   Himalaya and becomes arc-oblique in the western Himalaya, which is consistent with the

200   recent plate motion models by Kundu et al. (2014), where slip vectors mark the arc-normal

201   convergence in Central Himalaya (including GKH and Shimla zones) and oblique

202   convergence in Western Himalaya (Kangra-Chamba, Kishtwar and Kashmir zones). The

203   oblique convergence along western Himalaya produces pure-shear along the KF, located

204 northeast of this region and thrusting along the Himalayan intra-crustal thrusts. This is well

205 correlated with the arc-oblique stress orientations for Kangra-Chamba and Kishtwar zones in

206 the present study. Apparently, the change in convergence perturbs the regional stress field and

207 produces the arc-oblique stress field in the region.

208   The inversion of FM solutions in the epicentral region of 2005 Kashmir earthquake

209 (Hazara Syntaxis) and separately for its aftershocks shows little difference, suggestive of

210 similar stress orientations before, during and after the Kashmir earthquake (Figure 3,

211 Supplementary Figure S1). The stress orientations for the surrounding regions are not

212 compatible with this region, viz., WSW-ENE oriented compressional regime in the Kangra-

213 Chamba and Kishtwar regions and NNE-SSW oriented compressional regime in Hindu Kush

214 and NE-SW oriented strike-slip tectonics in Pamir region (Gahalaut & Rao, 2009). In an

215 earlier study, the stress orientations of the Kashmir earthquake and Hazara Syntaxis were

216 compared with that of the Himalaya, leading to apprehension over its origin being a

217 Himalayan earthquake (Gahalaut & Rao, 2009). However, those studies used earthquake FM

218 solutions for the entire Himalayan Arc that includes the earthquakes from Central and Eastern

219 Himalaya as well. In the present study, the stress orientations for the Kashmir earthquake

220 sequence and Hazara Syntaxis are found to be similar to that of the Central Himalaya (GKH

221 and Shimla zones), which strongly suggests that the Kashmir earthquake to be a Himalayan

222 earthquake. The optimal planes for the Hazara Syntaxis and for the aftershock sequence

223 (N=84) of Kashmir earthquake show shallow dip angles (21º and 22º, respectively), similar to

224 the mid-crustal ramp of the Central Himalaya (≤25º) (Table 1) (Gahalaut & Kalpna, 2001;

225 Prasath et al., 2017, 2019; Seeber et al., 1981). Further, the low R-value (0.4) for Hazara

226 Syntaxis and moderate value (0.6) for the aftershock sequence reveal a major role of σ1

227 during the aftershock activity and also suggest an interplay of the varying tectonic settings on

228 earthquake generation mechanisms in the region (Hindu Kush, Pamir and the Himalaya). The

229 low FC values (0.4-0.45) suggest that the faults in this region are weak and support the

230 presence of fluids, which is generally believed to affect the large earthquake generation

231 processes and control the aftershock genesis (Yu et al., 2019).

4.2. Strike-slip and extensional stress regimes

233 The stress fields in HSB and Western Tibet regions show distinctive stress regimes

234 with compressional and strike-slip tectonics, respectively with varying R-values (0.91 and 0.4,

235 respectively), suggesting predominant role of plate motion driven tectonic forces in HSB and

236 multiple tectonic forces in Western Tibet (Table 1). The optimal planes suggest that the faults

237 are steeper in Tibetan region with near-vertical dip angles in contrast to the faults with

238 shallow dip angle in HSB. The friction on the faults along HSB as well as Tibetan region have

239 been estimated to be ~0.7 and 0.64, which suggest the role of fluids in earthquake generation

240 and nucleation in IECZ (Table 1) (Prasath et al., 2017, 2019; Rawat et al., 2014; Kumar et al.,

241 2013, 2019).

242 The seismicity in the regions around KF is concentrated in the northwestern zone but

243 diffuse in the southeastern zone. We perform inversions separately for these two zones in

244 order to understand the stress distribution along this fault. The northwestern zone show strike-

245 slip tectonics with NE-SW oriented σ1 similar to that of the Himalayan regions and suggests

246 active nature of KF. However, the southeastern zone shows strike-slip tectonics with nearly

247 N-S oriented sub-horizontal σ1. Similarly, the R-value found to be varying from 0.39 in

248 northwest to 0.65 in southeast, consistent with the slip rates estimated for northwestern (5

249 mm/yr.) and southeastern (3.6 mm/yr.) parts of KF (Kundu et al., 2014). The data therefore

11

250 suggests the complex nature of stress field along KF, owing potentially to the association of

251 local and regional faults, viz., KCR, Karakax fault, Main Karakoram thrust and Longmu

252 Gozha fault. The FC values for northwestern and southeastern zones (0.71 and 0.82,

253 respectively) are close to the values estimated for Himalayan regions such as Kishtwar and

254 GKH (Table 1). The stress orientations along KCR show that the region is currently

255 experiencing oblique-slip tectonics with near-vertical σ2 and N-S oriented, sub-horizontal σ1,

256 which is compatible with that of geological, seismological and plate motion models,

257 suggesting that the KCR region is experiencing E-W directed trans-tension (DiPietro et al.,

258 2000; Dziewonski et al., 1981; Gahalaut and Kundu., 2012; Jade et al., 2014; Tapponnier et al.,

259 1981). Moreover, the moderate R-value (0.53) suggests involvement of multiple tectonic

260 forces in generation of earthquakes around this rift. The southeast KF and KCR zones are

261 found to be consistent as the inversion yields almost similar results and supports the previous

262 claims that the KCR may be extending deep into KF and segmenting it[25]. Hence, we

263 categorize these two zones as a single stress field. The Nanga Parbat Syntaxis, which is

264 located between the Kohistan Arc and Ladakh Arc show predominantly extensional tectonics,

265 ruling out any role of the Main Mantle Thrust (MMT) in generation of seismicity in this

266 region. Moreover, the optimal planes suggest the causative fault to be normal with steep dip

267 (~60º), further suggesting that the stress regime is controlled by the normal faulting along the

268 Kohistan Arc (DiPietro et al., 2000; Seeber & Pêcher, 1998). The moderate R-value (0.63)

269 suggests the reasonable involvement of multiple tectonic stresses (Table 1) similar to the

270 Hazara Syntaxis.

271

272

273   *4.3. State of stress fields*

274   Based on the detailed analysis of stress orientations, we classify the western IECZ into

275   six state of stress fields consistent with geomorphology, geology and plate motion models

276   (Figure 3). These are, (I) GKH-Shimla (ID 14), (II) Kangra-Chamba-Kishtwar (ID 15), (III)

277   Hazara Syntaxis (ID 5), (IV) Nanga Parbat Syntaxis (ID 7), (V) northwest KF (ID 8) and (VI)

278   southeast KF-KCR (ID 16) (Figures 3 and 4 and Supplementary Figure S1). Despite their

279   different tectonic setup, the stress fields I and III share similar properties with compressional

280   regime and arc-normal horizontal compressive stresses. However, their stress magnitudes

281   differ substantially (0.9 and 0.42 for GHK-Shimla and Hazara Syntaxis, respectively) owing

282   to their structural and tectonic association, where the Hazara Syntaxis located in the terminal

283   end of the Himalaya surrounded by Hindu Kush and Pamir regions in contrast to the GHK-

284   Shimla regions that are located entirely within the Himalaya. In contrast to these stress fields,

285   the stress field II shows compressional regime with arc-oblique horizontal stress field. The

286   stress field IV, i.e. Nanga Parbat Syntaxis shows predominantly extensional regime. While the

287   stress fields V and VI show strike-slip tectonic regime, the relative plate motion is the

288   dominant force in these regions too. The spatial distribution of stress fields shows a

289   decreasing trend in stress magnitude (R-value) from southeast (0.90 in GKH-Shimla) to

290   Kangra-Chamba-Kishtwar (0.72) and northwest (0.46 in Hazara Syntaxis). A similar trend has

291   been observed in the northeast with 0.52 for southeast KF-KCR and 0.39 for northeast KF.

292   The low stress magnitudes coincide with the regions having multiple tectonic forces involving

293   Hindu Kush, Pamir and the Himalaya in the northwestern end of the region (Hazara Syntaxis)

294   and local and regional faults, viz., KF, KXF and LGF in the northeastern part (Karakoram

295   Ranges).

5. Conclusion

296

297   Our study confirms that the western IECZ is characterized by a heterogeneous stress

298   field. This heterogeneity exists mainly because of the variation in the India-Eurasia

299   convergence, local and regional structures, multiple tectonic forces and the presence of fluids

300   in the region. Zone-wise analysis of focal mechanism solutions provide the following new

301   insights: (i) Arc-normal compression in Garhwal-Kumaun-Shimla region and arc-oblique

302   compression in Kangra-Chamba-Kishtwar region, (ii) Himalayan-type stress orientations for

303   Kashmir earthquake (2005) and Hazara Syntaxis, (iii) Pure extension at Nanga Parbat

304   Syntaxis, and (iv) Extension of the transverse feature KCR, with N-S trending $\sigma 1$, deep into

305   KF. From these inferences, we categorize the region into six state of stress fields. The

306   decreasing trend in stress magnitudes from the southeast to the northwest suggests the

307   presence of multiple tectonic forces towards northwestern (Hazara Syntaxis) and northeastern

308   (Karakoram) regions. The new results will be useful for simulation of geodynamic stress field,

309   earthquake nucleation processes and seismic hazard assessments.

310

14

317 catalog, published journal articles and it can be accessed collectively from the supplementary

318 tables or their respective sources, as mentioned in the article.

319

320 **Competing Interests**

321 The authors declare no competing interests.

322

323 **References**

324 1. Arora, B. R., Bansal, B. K., Prajapati, S. K., Sutar, A. K., & Nayak, S. (2017).

325 Seismotectonics and seismogenesis of Mw7. 8 Gorkha earthquake and its

326 aftershocks. *Journal of Asian Earth Sciences*, *133*, 2-11.

327 2. Arora, B. R., Gahalaut, V. K., & Kumar, N. (2012). Structural control on along-strike

328 variation in the seismicity of the northwest Himalaya. *Journal of Asian Earth*

329 *Sciences*, *57*, 15-24.

330 3. Avouac, J. P., Ayoub, F., Leprince, S., Konca, O., & Helmberger, D. V. (2006). The

331 2005, Mw 7.6 Kashmir earthquake: Sub-pixel correlation of ASTER images and seismic

332 waveforms analysis. *Earth and Planetary Science Letters*, *249*(3-4), 514-528.

333 4. Banerjee, P., & Bürgmann, R. (2002). Convergence across the northwest Himalaya from

334 GPS measurements. *Geophysical Research Letters*, *29*(13), 30-1.

335 5. Banerjee, P., Bürgmann, R., Nagarajan, B., & Apel, E. (2008). Intraplate deformation of

336 the Indian subcontinent. *Geophysical Research Letters*, *35*(18).

6. Baranowski, J., Armbruster, J., Seeber, L., & Molnar, P. (1984). Focal depths and fault plane solutions of earthquakes and active tectonics of the Himalaya. *Journal of Geophysical Research: Solid Earth*, *89*(B8), 6918-6928.

7. Chandra, U. (1978). Seismicity, earthquake mechanisms and tectonics along the Himalayan mountain range and vicinity. *Physics of the Earth and Planetary Interiors*, *16*(2), 109-131.

8. Chaudhury, H. M., Srivastava, H. N., & Rao, J. S. (1974). Seismotectonic investigations of the Himalayas. *Him. Geol*, *4*, 481-491.

9. D'Amico, S. (Ed.). (2018). *Moment Tensor Solutions: A Useful Tool for Seismotectonics*. Springer.

10. Das Gupta, A., Srivastava, H. N., & Basu, M. S. (1982). Source mechanism of earthquakes in Kangra–Chamba region of Himachal Pradesh, India. *Bull. Ind. Soc. Earthq. Tech*, *19*, 102-116.

11. DiPietro, J. A., Hussain, A., Ahmad, I., & Khan, M. A. (2000). The Main Mantle Thrust in Pakistan: its character and extent. *Geological Society, London, Special Publications*, *170*(1), 375-393.

12. Dziewonski, A. M., Chou, T. A., & Woodhouse, J. H. (1981). Determination of earthquake source parameters from waveform data for studies of global and regional seismicity. *Journal of Geophysical Research: Solid Earth*, *86*(B4), 2825-2852.

13. Ekström, G., Nettles, M., & Dziewoński, A. M. (2012). The global CMT project 2004–2010: Centroid-moment tensors for 13,017 earthquakes. *Physics of the Earth and Planetary Interiors*, *200*, 1-9.

16

359   14. Eugster, P., Thiede, R. C., Scherler, D., Stübner, K., Sobel, E. R., & Strecker, M. R.

360   (2018). Segmentation of the Main Himalayan Thrust Revealed by Low-Temperature

361   Thermochronometry in the Western Indian Himalaya. *Tectonics*, *37*(8), 2710-2726.

362   15. Gahalaut, K. and Rao, N.P., 2009. Stress field in the western Himalaya with special

363   reference to the 8 October 2005 Muzaffarabad earthquake. *Journal of seismology*, *13*(3),

364   p.371.

365   16. Gahalaut, V. K., & Kalpna. (2001). Himalayan mid-crustal ramp. *Current Science*, 1641-

366   1646.

367   17. Gahalaut, V. K., & Kundu, B. (2012). Possible influence of subducting ridges on the

368   Himalayan arc and on the ruptures of great and major Himalayan earthquakes. *Gondwana*

369   *Research*, *21*(4), 1080-1088.

370   18. Gephart, J. W., & Forsyth, D. W. (1984). An improved method for determining the

371   regional stress tensor using earthquake focal mechanism data: application to the San

372   Fernando earthquake sequence. *Journal of Geophysical Research: Solid Earth*, *89*(B11),

373   9305-9320.

374   19. Gansser, A. (1964). Geology of the Himalayas: London, Wiley Interscience, 289 pp.

375   20. Hazarika, D., Paul, A., Wadhawan, M., Kumar, N., Sen, K., & Pant, C. C. (2017).

376   Seismotectonics of the Trans-Himalaya, Eastern Ladakh, India: Constraints from moment

377   tensor solutions of local earthquake data. *Tectonophysics*, *698*, 38-46.

378   21. Hintersberger, E., Thiede, R. C., Strecker, M. R., & Hacker, B. R. (2010). East-west

379   extension in the NW Indian Himalaya. *Bulletin*, *122*(9-10), 1499-1515.

380   22. ISC (2019). International Seismological Centre, online bulletin, http://www.isc.ac.uk ,

381   Thatcham, United Kingdom.

23. Jade, S., Mukul, M., Gaur, V. K., Kumar, K., Shrungeshwar, T. S., Satyal, G. S., ... & Banerjee, S. (2014). Contemporary deformation in the Kashmir–Himachal, Garhwal and Kumaon Himalaya: significant insights from 1995–2008 GPS time series. *Journal of Geodesy*, *88*(6), 539-557.

24. Jade, S., Shrungeshwara, T. S., Kumar, K., Choudhury, P., Dumka, R. K., & Bhu, H. (2017). India plate angular velocity and contemporary deformation rates from continuous GPS measurements from 1996 to 2015. *Scientific reports*, *7*(1), 1-16.

25. Kanna, N., Gupta, S., & Prakasam, K. S. (2018). Micro-seismicity and seismotectonic study in Western Himalaya–Ladakh-Karakoram using local broadband seismic data. *Tectonophysics*, *726*, 100-109.

26. Kumar, N., Aoudia, A., Guidarelli, M., Babu, V. G., Hazarika, D., & Yadav, D. K. (2019). Delineation of lithosphere structure and characterization of the Moho geometry under the Himalaya–Karakoram–Tibet collision zone using surface-wave tomography. *Geological Society, London, Special Publications*, *481*(1), 19-40.

27. Kumar, N., Arora, B. R., Mukhopadhyay, S., & Yadav, D. K. (2013). Seismogenesis of clustered seismicity beneath the Kangra–Chamba sector of northwest Himalaya: constraints from 3D local earthquake tomography. *Journal of Asian Earth Sciences*, *62*, 638-646.

28. Kumar, N., Sharma, J., Arora, B. R., & Mukhopadhyay, S. (2009). Seismotectonic model of the Kangra–Chamba sector of northwest Himalaya: Constraints from joint hypocenter determination and focal mechanism. *Bulletin of the Seismological Society of America*, *99*(1), 95-109.

18

404   29. Kundu, B., Yadav, R. K., Bali, B. S., Chowdhury, S., & Gahalaut, V. K. (2014). Oblique

405   convergence and slip partitioning in the NW Himalaya: Implications from GPS

406   measurements. *Tectonics*, *33*(10), 2013-2024.

407   30. Leech, M. L. (2008). Does the Karakoram fault interrupt mid-crustal channel flow in the

408   western Himalaya?. *Earth and Planetary Science Letters*, *276*(3-4), 314-322.

409   31. Leech, M. L., Singh, S., Jain, A. K., Klemperer, S. L., & Manickavasagam, R. M. (2005).

410   The onset of India–Asia continental collision: early, steep subduction required by the

411   timing of UHP metamorphism in the western Himalaya. *Earth and Planetary Science*

412   *Letters*, *234*(1-2), 83-97.

413   32. Li, S., Wang, Q., Yang, S., Qiao, X., Nie, Z., Zou, R., ... & Chen, G. (2018). Geodetic

414   imaging mega-thrust coupling beneath the Himalaya. *Tectonophysics*, *747*, 225-238.

415   33. Mahajan, A. K., Thakur, V. C., Sharma, M. L., & Chauhan, M. (2010). Probabilistic

416   seismic hazard map of NW Himalaya and its adjoining area, India. *Natural*

417   *Hazards*, *53*(3), 443-457.

418   34. Mahesh, P., Gupta, S., Saikia, U. and Rai, S.S., 2015. Seismotectonics and crustal stress

419   field in the Kumaon–Garhwal Himalaya. *Tectonophysics*, *655*, pp.124-138.

420   35. Michael, A. J. (1987). Use of focal mechanisms to determine stress: a control

421   study. *Journal of Geophysical Research: Solid Earth*, *92*(B1), 357-368.

422   36. Molnar, P., & Chen, W. P. (1983). Focal depths and fault plane solutions of earthquakes

423   under the Tibetan plateau. *Journal of Geophysical Research: Solid Earth*, *88*(B2), 1180-

424   1196.

425 37. Molnar, P., & Lyon-Caent, H. (1989). Fault plane solutions of earthquakes and active
426   tectonics of the Tibetan Plateau and its margins. *Geophysical Journal*
427   *International*, *99*(1), 123-153.

428 38. Molnar, P., & Lyon-Caent, H. (1989). Fault plane solutions of earthquakes and active
429   tectonics of the Tibetan Plateau and its margins. *Geophysical Journal*
430   *International*, *99*(1), 123-153.

431 39. Molnar, P., & Tapponnier, P. (1977). The collision between India and Eurasia. *Scientific*
432   *American*, *236*(4), 30-41.

433 40. Mondal, S. K., Borghi, A., Roy, P. N. S., & Aoudia, A. (2016). GPS, scaling exponent
434   and past seismicity for seismic hazard assessment in Garhwal–Kumaun, Himalayan
435   region. *Natural Hazards*, *80*(2), 1349-1367.

436 41. Negi, S. S., Paul, A., Cesca, S., Kriegerowski, M., Mahesh, P., & Gupta, S. (2017).
437   Crustal velocity structure and earthquake processes of Garhwal-Kumaun Himalaya:
438   Constraints from regional waveform inversion and array beam
439   modeling. *Tectonophysics*, *712*, 45-63.

440 42. Nennewitz, M., Thiede, R. C., & Bookhagen, B. (2018). Fault activity, tectonic
441   segmentation, and deformation pattern of the western Himalaya on Ma timescales
442   inferred from landscape morphology. *Lithosphere*, *10*(5), 632-640.

443 43. Ni, J., & Barazangi, M. (1984). Seismotectonics of the Himalayan collision zone:
444   Geometry of the underthrusting Indian plate beneath the Himalaya. *Journal of*
445   *Geophysical Research: Solid Earth*, *89*(B2), 1147-1163.

446   44. Parija, M. P., Kumar, S., Tiwari, V. M., Rao, N. P., Kumar, N., Biswal, S., & Singh, I.

447   (2018). Microseismicity, tectonics and seismic potential in the Western Himalayan

448   segment, NW Himalaya, India. *Journal of Asian Earth Sciences*, *159*, 1-16.

449   45. Paul, H., Priestley, K., Powali, D., Sharma, S., Mitra, S., & Wanchoo, S. (2018).

450   Signatures of the existence of frontal and lateral ramp structures near the Kishtwar

451   Window of the Jammu and Kashmir Himalaya: evidence from microseismicity and

452   source mechanisms. *Geochemistry, Geophysics, Geosystems*, *19*(9), 3097-3114.

453   46. Paul, J., Bürgmann, R., Gaur, V. K., Bilham, R., Larson, K. M., Ananda, M. B., ... &

454   Kumar, D. (2001). The motion and active deformation of India. *Geophysical Research

455   Letters*, *28*(4), 647-650.

456   47. Phillips, R. J., Parrish, R. R., & Searle, M. P. (2004). Age constraints on ductile

457   deformation and long-term slip rates along the Karakoram fault zone, Ladakh. *Earth and

458   Planetary Science Letters*, *226*(3-4), 305-319.

459   48. Prasath, R. A., Paul, A., & Singh, S. (2017). Upper crustal stress and seismotectonics of

460   the Garhwal Himalaya using small-to-moderate earthquakes: Implications to the local

461   structures and free fluids. *Journal of Asian Earth Sciences*, *135*, 198-211.

462   49. Prasath, R. A., Paul, A., & Singh, S. (2019). Earthquakes in the Garhwal Himalaya of the

463   Central Seismic Gap: A Study of Historical and Present Seismicity and Their

464   Implications to the Seismotectonics. *Pure and Applied Geophysics*, *176*(11), 4661-4685.

465   50. Ram, V. S., Kumar, D., & Khattri, K. N. (2005). The 1986 Dharamsala earthquake of

466   Himachal Himalaya–estimates of source parameters, average intrinsic attenuation and site

467   amplification functions. *Journal of seismology*, *9*(4), 473-485.

468   51. Rastogi, B. K. (1974). Earthquake mechanisms and plate tectonics in the Himalayan
469   region. *Tectonophysics*, *21*(1-2), 47-56.

470   52. Rawat, G., Arora, B. R., & Gupta, P. K. (2014). Electrical resistivity cross-section across
471   the Garhwal Himalaya: Proxy to fluid-seismicity linkage. *Tectonophysics*, *637*, 68-79.

472   53. Sapkota, S. N., Bollinger, L., Klinger, Y., Tapponnier, P., Gaudemer, Y., & Tiwari, D.
473   (2013). Primary surface ruptures of the great Himalayan earthquakes in 1934 and
474   1255. *Nature Geoscience*, *6*(1), 71-76.

475   54. Seeber, L., & Pêcher, A. (1998). Strain partitioning along the Himalayan arc and the
476   Nanga Parbat antiform. *Geology*, *26*(9), 791-794.

477   55. Seeber, L., Armbruster, J. G., & Quittmeyer, R. C. (1981). Seismicity and continental
478   subduction in the Himalayan arc. *Zagros Hindu Kush Himalaya Geodynamic*
479   *Evolution*, *3*, 215-242.

480   56. Singh, R., Prasath, R. A., Paul, A., & Kumar, N. (2018). Earthquake swarm of Himachal
481   Pradesh in northwest Himalaya and its seismotectonic implications. *Physics of the Earth*
482   *and Planetary Interiors*, *275*, 44-55.

483   57. Srinagesh, D., Singh, S. K., Suresh, G., Srinivas, D., Pérez-Campos, X., & Suresh, G.
484   (2018). A study of Guptkashi, Uttarakhand earthquake of 6 February 2017 (M w 5.3) in
485   the Himalayan arc and implications for ground motion estimation. *Journal of*
486   *Seismology*, *22*(3), 789-803.

487   58. Tandon, A. N., & Srivastava, H. N. (1975). Focal mechanisms of some recent Himalayan
488   earthquakes and regional plate tectonics. *Bulletin of the Seismological Society of*
489   *America*, *65*(4), 963-969.

490   59. Tapponnier, P., Mercier, J.L., Armijo, R., Tonglin, H. and Ji, Z., 1981. Field evidence for
491   active normal faulting in Tibet. *Nature*, *294*(5840), pp.410-414.

492   60. Thakur, V. C. (1992). Geology of western Himalaya. *Physics and Chemistry of the*
493   *Earth*, *19*, 1-355.

494   61. Thakur, V. C., & Jayangondaperumal, R. (2015). Seismogenic active fault zone between
495   2005 Kashmir and 1905 Kangra earthquake meizoseismal regions and earthquake hazard
496   in eastern Kashmir seismic gap. *Current Science (00113891)*, *109*(3).

497   62. Vavryčuk, V., 2014. Iterative joint inversion for stress and fault orientations from focal
498   mechanisms. *Geophysical Journal International*, *199*(1), pp.69-77.

499   63. Verma, M., Sutar, A. K., Bansal, B. K., Arora, B. R., & Bhat, G. M. (2015). MW 4.9
500   earthquake of 21 August, 2014 in Kangra region, Northwest Himalaya: Seismotectonics
501   implications. *Journal of Asian Earth Sciences*, *109*, 29-37.

502   64. Verma, R. K., & Sekhar, C. C. (1986). Focal mechanism solutions and nature of plate
503   movements in Pakistan. *Journal of geodynamics*, *5*(3-4), 331-351.

504   65. Wallis, D., & Searle, M. P. (2019). Spatial and Temporal Distributions of Deformation in
505   Strike-Slip Faults: The Karakoram Fault in the India-Asia Collision Zone. In *Transform*
506   *Plate Boundaries and Fracture Zones* (pp. 271-300). Elsevier.

507   66. Yadav, D. K., Hazarika, D., & Kumar, N. (2016). Seismicity and stress inversion study in
508   the Kangra–Chamba region of north-west Himalaya. *Natural Hazards*, *82*(2), 1393-1409.

509   67. Yadav, D. K., Kumar, N., Hazarika, D., Yadav, D. N., & Wadhawan, M. (2017).
510   Seismicity and Tectonics of Kinnaur Himalaya and adjoining region inferred from focal
511   mechanism solutions and stress tensor inversion. *HIMALAYAN GEOLOGY*, *38*(1), 49-55.

23

68. Yu, Z., Zhao, D., Li, J., Huang, Z., Nishizono, Y., & Inakura, H. (2019). Stress field in the 2016 Kumamoto earthquake (M 7.3) area. *Journal of Geophysical Research: Solid Earth*, *124*(3), 2638-2652.

Author Contributions

R.A.P., B.K.B., and M.V. have conceived the research problem. R.A.P. performed data compilation and analysis. R.A.P., B.K.B., and M.V. interpreted the results. R.A.P. drafted all the figures and prepared the first draft of the manuscript. R.A.P., B.K.B., and M.V. have finalized the manuscript.

Figure Legends

Figure 1. **The western India-Eurasia Collision Zone, its Structure, Tectonics and Seismicity.** (a) Map of the study area along with the major geological structure and tectonic elements (Thakur, 1992; Thakur & Jayamgondaperumal, 2005; Wallis & Searle, 2019). (b) Epicentral locations of FM solutions used in the present study with the background seismicity from the catalog of International Seismological Center (ISC). Acronyms: AK-Almora Klippen, BBF- Balakot Bagh Fault, HFT-Himalayan Frontal Thrust, HHC-Higher Himalayan Crystallines, HS-Hazara Syntaxis, IGP-Indo Gangetic Plains, ITS-Indus Tsangpo Suture, JF-Jhelum Fault, KB-Kashmir Basin, KCR-Kaurik Chango Rift, KF-Karakoram Fault, KLRW-Kullu-Larji-Rampur Window, KW-Kishtwar Window, KXF-Karakax Fault, LGF-Longmu Gozha Fault, LH-Lesser Himalaya, MBT-Main Boundary Thrust, MCT-Main Central Thrust, MKT-Main Karakoram Thrust, MMT-Main Mantle Thrust, NPS-Nanga Parbat Syntaxis, SH-

534 Sub Himalaya, SRT-Salt Range Thrust, STD-Southern Tibetan Detachment, TH-Tethyan

535 Himalaya, TP-Tibetan Plateau.

536

537 Figure 2. **Earthquake Focal Mechanism solutions used in the present study.** Figure shows

538 the Earthquake FM solutions along with the seismotectonic zones, viz., (1) Garhwal-Kumaun

539 Himalaya, (2) Shimla, (3) Kangra-Chamba, (4) Kishtwar, (5) Hazara Syntaxis, (6) Nanga

540 Parbat Syntaxis, (7) Northwest Karakoram Fault, (8) Southeast Karakoram Fault and (9)

541 Kaurik Chango Rift. Acronyms are similar to those given in Fig. 1

542

543 Figure 3. **Major results of the study.** (a) Principle stress axes from the stress inversions

544 plotted with the respective zones. Inset-A shows the classification of stress fields (1-6) for the

545 western IECZ. Acronyms are similar to as given in Fig. 1

546

547 Figure 4. **Stress inversion plots for six stress fields categorized in the present study**. (a)

548 Principle stress and P/T axes, (b) Confidence of the stress axes, (c) Mohr circle diagram and

549 (d) Shape ratio 'R'.

550

551

552

553

Table(s)

555 Table 1. Results of stress inversions using earthquake focal mechanisms in the western IECZ.

ID	Zone code	Zone	Nodal planes used	Stress Orientations (Az/Pl ±Error*)			Principle FMs S1/D1/R1, S2/D2/R2†	R	μ
				Sigma 1	Sigma 2	Sigma 3			
1	1	Garhwal-Kumaun Himalaya	106	212/19 ±05.5	114/23 ±25.6	337/60 ±25.3	095/53/060, 004/25/162	0.93± 0.19	0.66
2	2	Shimla	40	208/19 ±05.7	109/25 ±19.1	331/58 ±19.1	088/52/058, 004/26/166	0.85± 0.17	0.70
3	3	Kangra-Chamba	54	248/02 ±11.1	157/12 ±17.3	346/78 ±17.2	130/25/060, 009/22/124	0.62± 0.11	1.20
4	4	Khistwar Window	66	233/10 ±03.3	324/08 ±06.8	092/78 ±06.7	155/35/103, 299/17/064	0.78± 0.06	0.85
5	5a	Hazara Syntaxis	114	212/10 ±05.7	121/06 ±05.3	360/78 ±03.5	115/45/081, 315/25/105	0.46± 0.04	0.40
6	5b	Aftershocks of 2005 Kashmir EQ	84	219/12 ±07.2	127/03 ±13.3	025/78 ±13.7	125/45/086, 315/21/098	0.60± 0.07	0.45
7	6	Nanga Parbat Syntaxis	14	083/83 ±23.5	249/07 ±29.6	339/02 ±20.7	245/60/-097, 073/57/-082	0.63± 0.28	0.50
8	7	Northwest KF	26	221/50 ±38.5	040/40 ±37.5	130/01 ±24.4	022/70/-134, 239/69/-046	0.39± 0.29	0.71
9	8	Southeast KF	26	185/17 ±09.6	067/57 ±09.6	284/28 ±06.4	039/73/029, 345/57/-175	0.65± 0.10	0.82
10	9	KCR	28	358/30 ±10.1	195/59 ±37.7	092/07 ±37.6	023/85/-031, 161/72/-155	0.53± 0.15	0.95
11	HSB	Himalayan Seismic Belt	266	210/19 ±03.1	110/27 ±15.5	331/56 ±15.5	086/51/055, 015/26/175	0.91± 0.07	0.92
12	NHSB	North of HSB (Tibet)	116	205/06 ±07.4	047/83 ±07.2	296/03 ±03.9	234/89/-007, 357/85/-176	0.40± 0.06	0.64
13	All dataset	Whole region	490	214/13 ±02.0	121/11 ±13.3	353/73 ±13.3	108/41/073, 342/17/132	0.87± 0.03	0.77
14	1+2	Garhwal-Kumaun-Shimla	146	210/19 ±03.0	110/27 ±20.0	331/56 ±20.1	086/51/055, 015/27/176	0.90± 0.08	0.91
15	3+4	Kangra-Chamba-Khistwar	120	237/08 ±03.5	146/04 ±07.8	032/81 ±07.0	140/32/083, 339/16/104	0.72± 0.03	0.94
16	8+9	Southeast-KF and KCR	54	180/06 ±13.9	057/79 ±15.8	271/09 ±9.04	030/85/010, 332/79/-179	0.52± 0.09	0.64

556 *Az-Azimuth, Pl-Plunge, S1/S2-Strike 1 and 2, D1/D2-Dip 1 and 2, R1/R2-Rake 1 and 2, R-Shape ratio and μ-*

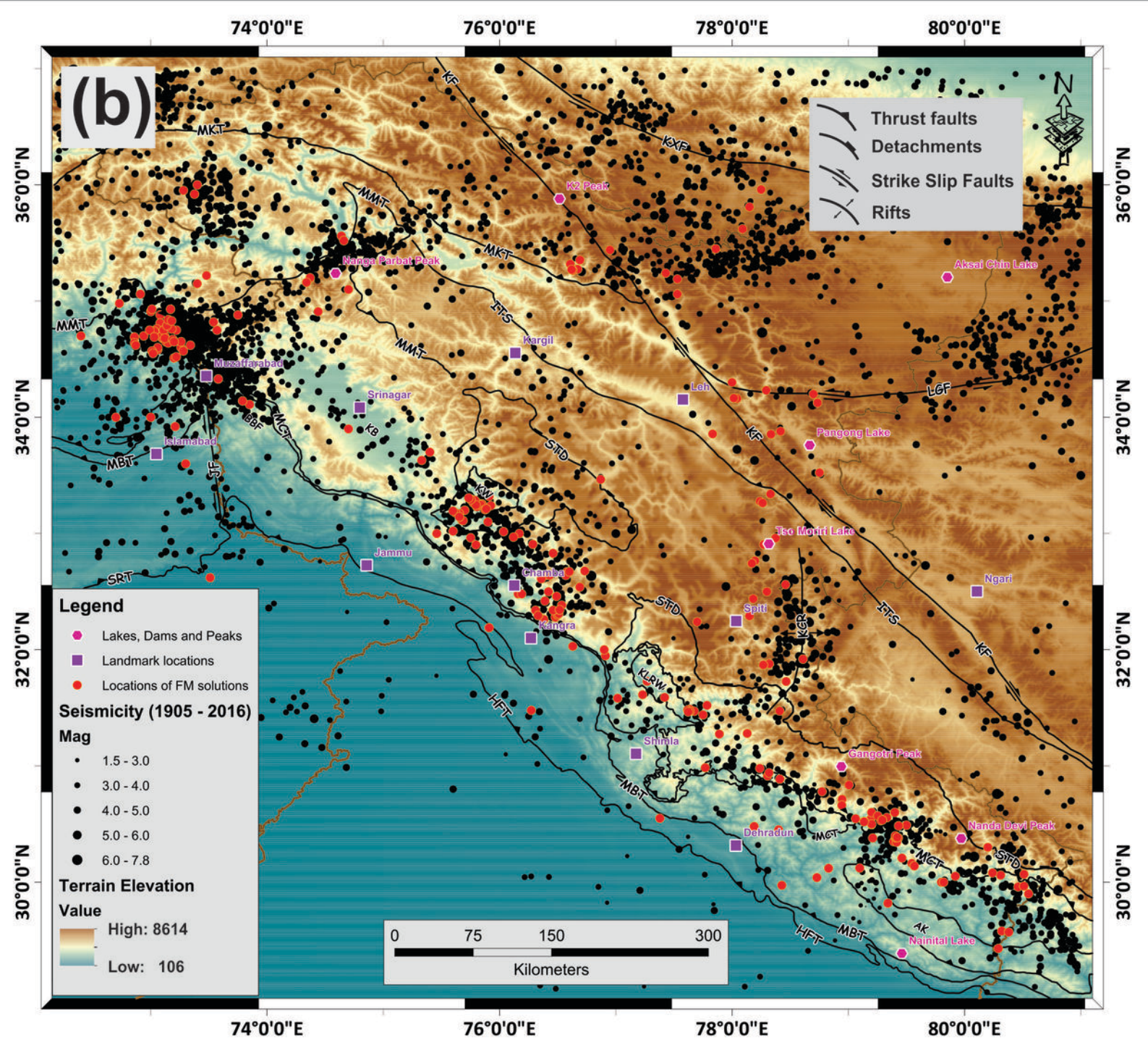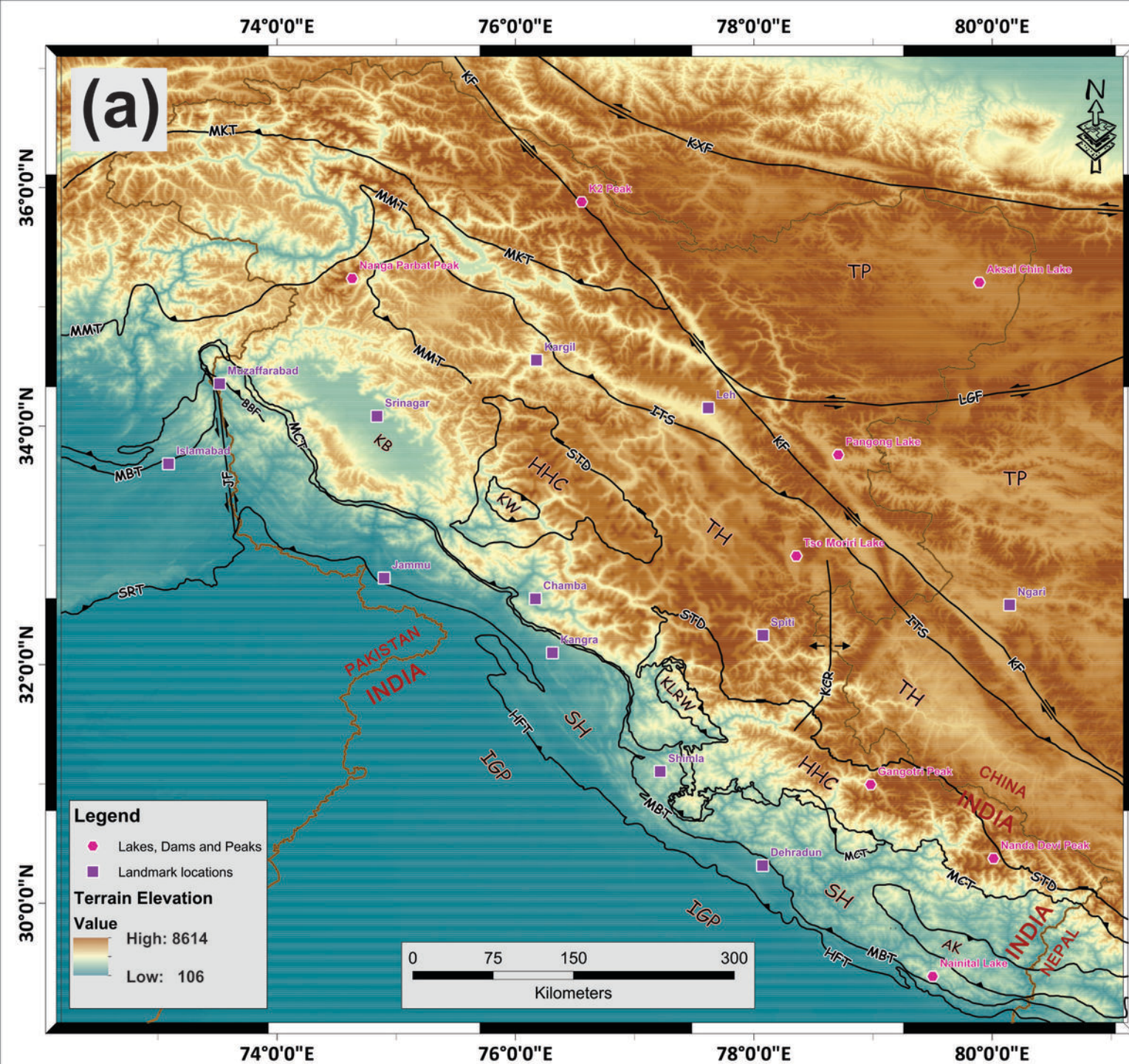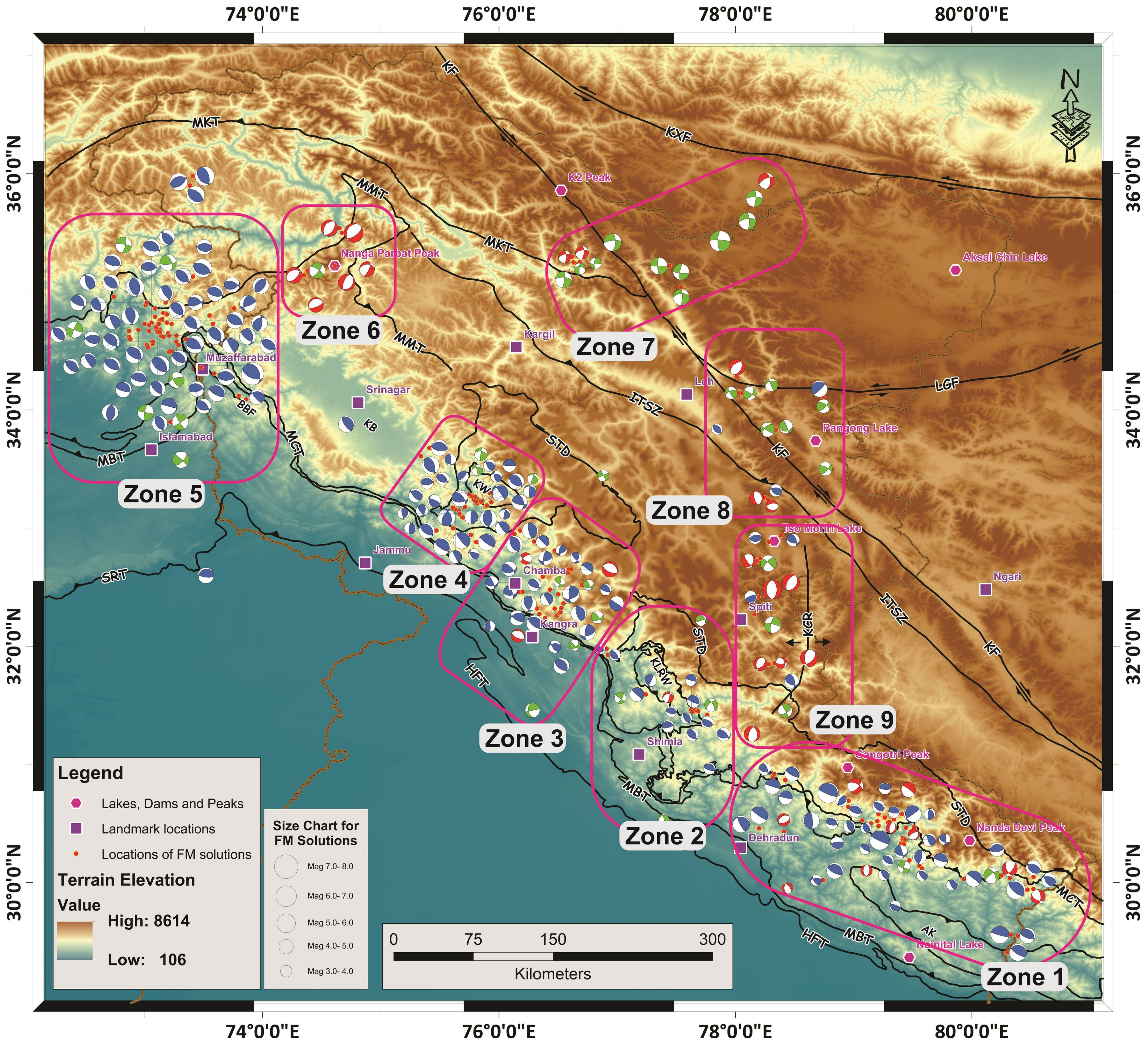557 *Friction Coefficient. *Errors are common for both Azimuth and Plunge values.*
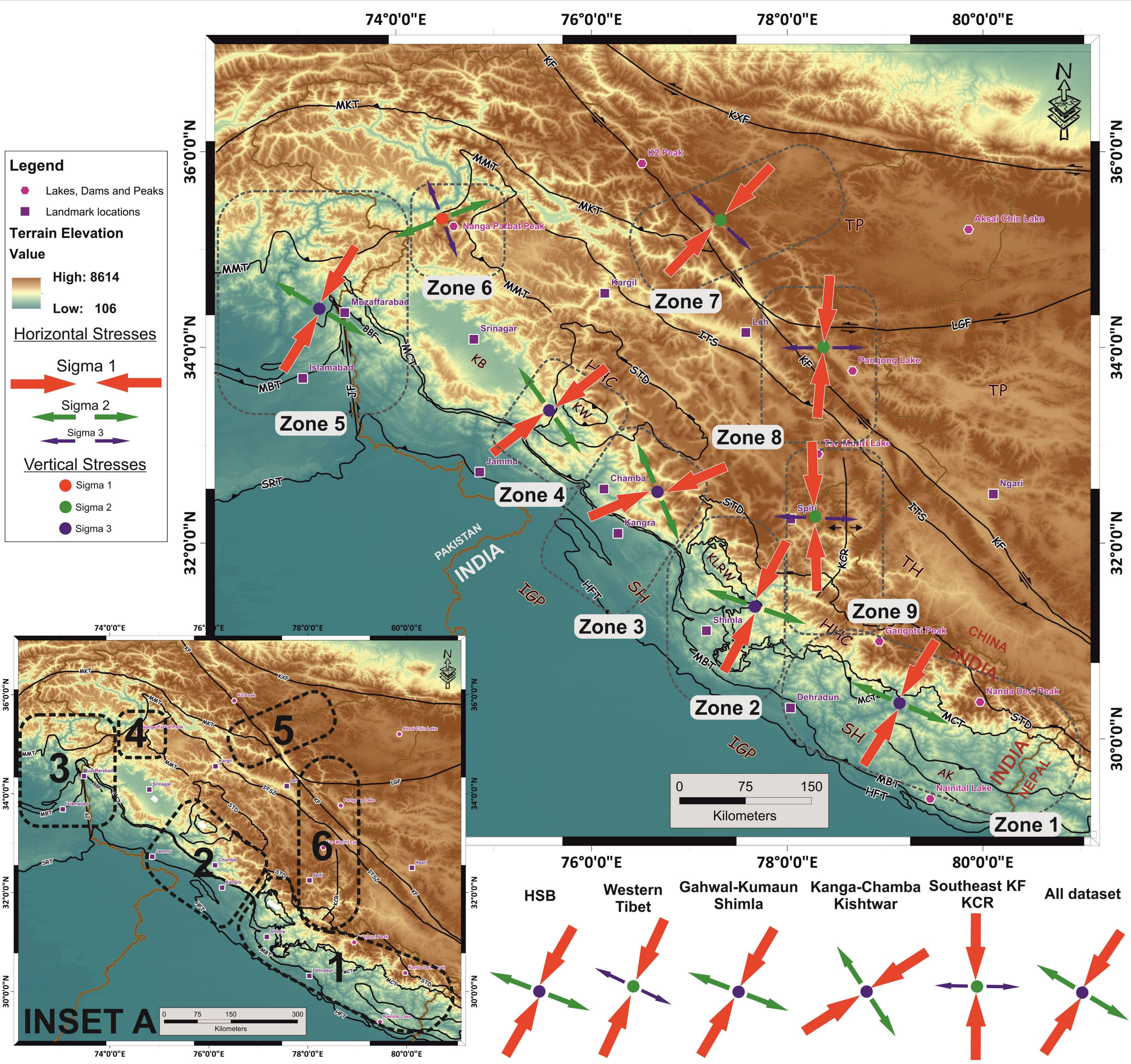
Figure 1.

Figure 2.

Figure 3.

Figure 4.

Stress Field I — (a), (b), (c), (d) R=0.91 ±0.08

Stress Field II — (a), (b), (c), (d) R=0.72 ±0.03

Stress Field III — (a), (b), (c), (d) R=0.46 ±0.04

Stress Field IV — (a), (b), (c), (d) R=0.63 ±0.28

Stress Field V — (a), (b), (c), (d) R=0.39 ±0.29

Stress Field VI — (a), (b), (c), (d) R=0.52 ±0.09